Stiffness Modeling of Industrial Robots for Deformation Compensation in Machining

Ulrich Schneider[1], Mahdi Momeni-K[1], Matteo Ansaloni[2] and Alexander Verl[1]

***Abstract*— In robotic machining applications, the precision of the robot is of great importance. In heavy machining process, the lower stiffness of industrial robots results in greater position errors than that of the CNC machine executing the same process. In this contribution, a new stiffness model with 36 degrees of freedom and nonlinear descriptions are presented together with a new identification method. Experimental results outline the potential of the model in machining application.**

I. INTRODUCTION

Industrial manipulators are traditionally used for the execution of repetitive tasks such as welding, handling and painting, while CNC machines are used in machining tasks where the external force applied to the end-effector is not negligible any more. However, due to the adaptability, flexibility, higher manoeuvrability, a bigger workspace and relatively low cost of the industrial robots, they could be a better option in industrial machining. Despite this useful features, inherent robots accuracy issues limits industrial robots usage in high precision machining applications, and consequently few successful implementation are achieved within the manufacture industry. According to Schneider [1] sources of errors in robot machining can be classified in three categories: 1) Environment dependent errors, 2) Robot dependent errors (geometrical and non-geometrical errors), and 3) Process dependent errors.

A load applied on a body changes the geometry of the body which is known as deformation or compliant displacement. Consequently, the stiffness of a body can be defined as the amount of force that can be applied per unit of compliant displacement of the body [2], or the ratio of a steady force acting on a deformable elastic medium to the resulting displacement [3].

The main reason preventing the adoption of industrial manipulators in heavy milling applications, in favour of standard CNC machines, is the fact that joints compliance affects negatively the overall manipulator stiffness measured at the Tool Center Point (TCP). As a result, the externally exerted force to the robot end-effector due to the interaction between the tooltip and the workpiece can deform the manipulator which in turn, results in positioning errors. The values of the machining forces depend on the process parameters: spindle speed, axial depth-of-cut, radial depth-of-cut and chip load. In heavy machining the deformation and the positioning error rise with the external forces. Therefore the deformation must be accurately compensated in order to achieve higher accuracy in positioning.

Previous approaches to increasing the position accuracy are primarily based on kinematic calibration [4]-[6] and stiffness modelling of the manipulator [7]-[10]. Kinematic calibration approaches determine kinematic parameters accurately. However, applying solely these approaches is not enough for increasing the accuracy in milling processes as the body deformation is not considered in such methods. In stiffness compensation methods, the robot stiffness matrix is identified offline based on experimental data and then, a proper online position controller is applied considering that the deformation due to the process forces is provided using a stiffness model.

In the Literature, the methods adopted to compensate for the robot deformation can be classified as model- and sensor- based methods. While the former methods use an already identified model to predict the robot deformation and subsequently modify the robot position reference [7]-[10], the sensor based methods either measure the deformation inducing the position error [11] or/and the tooltip position is retrieved from high precision 3D or 6D position measurement sensors, the measured error is used in the control loop to adjust the reference position accordingly [12]. Sensor based compensation methods require higher implementation efforts and hardware costs, mainly due to the costs of sensors, than model-based methods; but, on the other hand, they offer higher position accuracy. The main limitations of these methods are the disturbance rejection bandwidth at the robot end-effector, communication delays for sensor data and the noise in the measurements.

In model based approaches, the deformation of the body corresponding to the externally exerted force is measured provided that the stiffness matrix has been identified offline. Several experimental configurations can be devised in order to apply and measure the wrench, i.e. force and torque, on robot TCP. In paper [8], Authors use a force/torque sensor mounted on a tool. The external load is generated using a wire suspended between the robot tool and an air cylinder that can be adjusted to vary the force magnitude. Zhang [13] uses a more simple method where only the gravity from an external known load is used.

To compute the compliant displacement, different methods have been proposed which are based on spring equation. In [14], joint stiffness matrix is formulated. In [15], the formulation was developed and the conservative congruence transformation (CCT) was proposed.

[1]U. Schneider, M. Momeni-K and A. Verl are with Fraunhofer Institute for Manufacturing Engineering and Automation (IPA), Nobelstrasse 12, D-70569 Stuttgart, Germany. All correspondence should be addressed to Ulrich Schneider, E-mail: ulrich.schneider@ipa.fraunhofer.de

[2]M. Ansaloni is with Department of Engineering Enzo Ferrari, University of Modena, Strada Vignolese 905 - 41125 Modena, Italy

This contribution is organized as follows: An introduction to robot modeling and robot machining is given in Section I. Section II describes the developed stiffness modeling. The identification of the developed stiffness model is presented in Section III. Section IV demonstrates the quality of the model and the potential for robotic machining using a model-based compensation approach. Section V validates the developed methods in machining application followed by conclusions in Section VI.

II. ROBOT DEFORMATION MODELLING

Generally speaking, a multybody system acted upon by external loads deforms because of its compliance. Particularly within a robot, components like gearboxes, motors, links and other transmission elements are the major sources of compliance which contribute to the deformation.

In general, the purpose of the stiffness analysis is to define the stiffness of the overall system through the derivation of a stiffness matrix that relates the compliant displacement $\mathbf{\Delta X} = [\Delta x\ \Delta y\ \Delta z\ \Delta\varphi\ \Delta\psi\ \Delta\theta]^T$ of the end-effector frame due to the external wrench $\mathbf{W} = [F_x\ F_y\ F_z\ T_x\ T_y\ T_z]^T$ acting on it, where Δx, Δy, and Δz are the deviations in robot end-effector position and $\Delta\varphi$, $\Delta\psi$, and $\Delta\theta$ are the deviations in Euler angles due to the external wrench $\mathbf{W}$; F and T also represent the *Forces* and *Torques* along the x-, y-, and z-axis. The relationship between the vector of the compliant displacements $\mathbf{\Delta X}$ and external wrench $\mathbf{W}$ in reference frame $o - xyz$ can be written as:

$$\mathbf{W} = \mathbf{K}\ \mathbf{\Delta X} \tag{1}$$

where $\mathbf{K}_{6\times6}$ is called the Cartesian stiffness matrix. It is worth noting that $\mathbf{K}$ depends on the choice of the reference frame in which $\mathbf{\Delta X}$ and $\mathbf{W}$ are defined. As a result, if one defines the new reference frame $o'-x'y'z'$, Eq. 1 will change to $\mathbf{W}' = \mathbf{K}'\ \mathbf{\Delta X}'$ where in general $\mathbf{K} \neq \mathbf{K}'$. However, $\mathbf{W}'$ and $\mathbf{\Delta X}'$ can be related to $\mathbf{W}$ and $\mathbf{\Delta X}$ using the following equations:

$$\begin{cases} \mathbf{W}' = \mathbf{A}\ \mathbf{W} \\ \mathbf{\Delta X}' = \mathbf{a}\ \mathbf{\Delta X} \end{cases} \tag{2}$$

where:

$$\begin{cases} \mathbf{A} = \begin{bmatrix} {}^{o'}\mathbf{R}_o & \mathbf{0}_{3\times3} \\ {}^{o'}\mathbf{P}_o \times {}^{o'}\mathbf{R}_o & {}^{o'}\mathbf{R}_o \end{bmatrix} \\ \mathbf{a} = \begin{bmatrix} {}^{o'}\mathbf{R}_o & \mathbf{0}_{3\times3} \\ \mathbf{0}_{3\times3} & {}^{o'}\mathbf{R}_o \end{bmatrix} \end{cases} \tag{3}$$

where ${}^{o'}\mathbf{R}_o$ and ${}^{o'}\mathbf{P}_o$ are the rotation and position matrices representing the orientation of the frame $o - xyz$ w.r.t the frame $o' - x'y'z'$, respectively.

Using Eq. 2, it is also possible to find out the external wrench applied to each link of a general industrial manipulator. In other words, expanding Eq. 2, one can easily show that for each component of the robot the following equation holds:

$$\begin{cases} {}^{j}\mathbf{F}_j = {}^{j}\mathbf{R}_i\ {}^{i}\mathbf{F}_i \\ {}^{j}\mathbf{T}_j = {}^{j}\mathbf{R}_i\ ({}^{i}\mathbf{F}_i \times {}^{i}\mathbf{P}_j + {}^{i}\mathbf{T}_i) \end{cases} \tag{4}$$

where ${}^{i}\mathbf{P}_j$ and ${}^{j}\mathbf{R}_i$ are the position of the origin of coordinate frame j w.r.t frame i and rotation of coordinate frame i w.r.t frame j, respectively.

Consequently, by using equations 1 and 4, it is then possible to measure the compliant displacement of the origins of the coordinate systems attached to each component. Having found the deviation of the origins of all 6 coordinate frames due to the external wrench, it is possible to calculate the new homogeneous transformation matrices corresponding to each component, considering the change in joint variables due to the external wrench.

To measure the total compliant displacement, it is possible to use the forward kinematics:

$${}^{0}\mathbf{T}'_6 = {}^{0}\mathbf{T}'_1 \times {}^{1}\mathbf{T}'_2 \times {}^{2}\mathbf{T}'_3 \times {}^{3}\mathbf{T}'_4 \times {}^{4}\mathbf{T}'_5 \times {}^{5}\mathbf{T}'_6 \tag{5}$$

where ${}^{i-1}\mathbf{T}'_i, i = 1, ..., 6$ are the transformation matrices corresponding to the new joint variables. As a result, the total compliant displacement of the robot end-effector can be calculated by comparing the ${}^{0}\mathbf{T}_6$ and ${}^{0}\mathbf{T}'_6$, where ${}^{0}\mathbf{T}_6$ is the transformation matrix before the external forces are exerted. This means that $\mathbf{\Delta P}$ and $\mathbf{\Delta R}$ represent the total compliant displacement of the robot end-effector where:

$$\begin{cases} \mathbf{\Delta P} = {}^{0}\mathbf{P}_6 - {}^{0}\mathbf{P}'_6 \\ \mathbf{\Delta R} = {}^{0}\mathbf{R}_6^{-1\,0}\mathbf{R}'_6 \end{cases} \tag{6}$$

It is worth noting that, if desired, the deflection of the origin of each joint can be calculated by comparing the initial unloaded transformation matrix with the loaded transformation matrix for the corresponding serial kinematic chain. In other words, the generalized form of Eq. 6 can be used to calculate the deflection of each joint due to the external wrench:

$$\begin{cases} \mathbf{\Delta P} = {}^{0}\mathbf{P}_i - {}^{0}\mathbf{P}'_i \\ \mathbf{\Delta R} = {}^{0}\mathbf{R}_i^{-1\,0}\mathbf{R}'_i \end{cases} \tag{7}$$

where i stands for the desired joint. Equation 7 can also be used to find out how accurate the deflection of each joint is calculated by comparing it with the measured frames under load (compare Section III).

III. STIFFNESS IDENTIFICATION

A. Mathematical Formulation

The evaluation of stiffness matrix $\mathbf{K}$ in Eq. 1 can be carried out using a least square approach, provided that the full wrench vector and the full pose displacement, i.e. displacement in position and orientation, can be measured in the same coordinate frame.

Considering the frame $o - xyz$, the external wrench and the corresponding deformation in this frame can be expressed as:

$$\begin{cases} \mathbf{W} = [F_x\ F_y\ F_z\ T_x\ T_y\ T_z]^T \\ \mathbf{\Delta X} = [\Delta x\ \Delta y\ \Delta z\ \Delta\varphi\ \Delta\psi\ \Delta\theta]^T \end{cases} \tag{8}$$

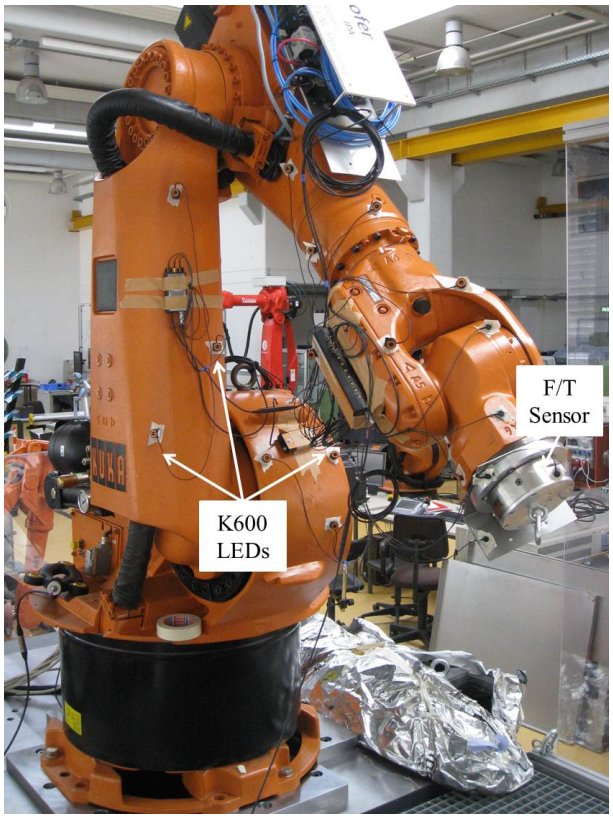

Fig. 1: Experimental setup

The fitting error is expressed as:

$$\mathbf{e} = \sum_{i=1}^{N} \mathbf{e}_i^T \, \mathbf{e}_i = \sum_{i=1}^{N} \mathbf{W}_i \, \mathbf{W}_i^T - (\sum_{i=1}^{N} \mathbf{\Delta X}_i \, \mathbf{W}_i^T)^T \, \mathbf{K} \quad (9)$$

Equation 1 can be re-written in the following form:

$$\mathbf{W}^T = \mathbf{\Delta X}^T \, \mathbf{K}^T \quad (10)$$

The objective is to minimize:

$$S(\mathbf{K}) = \|\mathbf{W}^T - \mathbf{\Delta X}^T \, \mathbf{K}^T\|^2 \quad (11)$$

Equation 11 is equivalent to:

$$\begin{aligned} S(\mathbf{K}) &= (\mathbf{W}^T - \mathbf{\Delta X}^T \, \mathbf{K}^T)^T \, (\mathbf{W}^T - \mathbf{\Delta X}^T \, \mathbf{K}^T) \\ &= \mathbf{W}\mathbf{W}^T - \mathbf{W}\mathbf{\Delta X}^T\mathbf{K}^T \\ &\quad - \mathbf{K}\mathbf{\Delta X}\mathbf{W}^T + \mathbf{K}\mathbf{\Delta X}\mathbf{\Delta X}^T\mathbf{K}^T \end{aligned} \quad (12)$$

Differentiating the resulting equation with respect to $\mathbf{K}$ and equating to zero gives:

$$-2\mathbf{\Delta X}\mathbf{W}^T + 2\mathbf{\Delta X}\mathbf{\Delta X}^T\mathbf{K}^T = 0 \quad (13)$$

which gives:

$$\Rightarrow \mathbf{K}^T = (\mathbf{\Delta X}\mathbf{\Delta X}^T)^{-1}\mathbf{\Delta X}\mathbf{W}^T \quad (14)$$

Considering a set of N measurements, the least square solution of the Cartesian stiffness matrix $\hat{\mathbf{K}}$ is:

$$\hat{\mathbf{K}}^T = (\sum_{i=1}^{N} \mathbf{\Delta X}_i \, \mathbf{\Delta X}_i^T)^{-1} \, (\sum_{i=1}^{N} \mathbf{\Delta X}_i \, \mathbf{W}_i^T) \quad (15)$$

Based on this formulation stiffness is identified from experimental data in Section III-C.

B. Experimental Setup

Figure 1 shows an experimental setup for identifying the stiffness of a KUKA KR 125 industrial manipulator and robotic machining.The KR 125 together with a K600 optical measurement system from Nikon Metrology [16] and a Chopper 3300 spindle from Alfred Jäger are combined on a 14 t machine bed. The sensing of a series of LEDs with three cameras in an appropriate workspace allowes to measure several frames with an accuracy of $\pm 90\,\mu$m in a cycle time up to 1 kHz. The possibility to attach redundant LEDs is essential for reduction of measurement noise and for the provision of a constant measurement signal while shadowing LEDs by robot movements.

The measurement of the external wrench is performed using a ATI Theta force/torque sensor theta 2500/400 [17]; this sensor is mounted on the robot flange. To measure the deformation, the K600 optical measurement system is used. The external wrench in different magnitude is exerted to the robot end-effector in different directions.

It should be pointed out that stiffness matrix could be identified at a single robot configuration by changing the wrench magnitude and direction. Anyway, performing the identification experiment in different configurations not only allow the verification of the deformation model, but also the reduction of the identification error through averaging.

To have a better understanding of the deformation, the external load attached to the robot end-effector varies from $-max$ to max payload at each configuration, where $-max$ implies the max payload in the negative direction of the x-, y-, or z-axis of the end-effector frame. Based on the set of four LEDs (with each of them providing 3D information) a complete 6D frame can be computed. It should also be noted that prior to the wrench measurement at each load condition, a few seconds are imposed in order for the deformation to be stabilized. Each load scenario is captured with a set of 10 measurements in order to minimize measurement errors. Afterwards, the pose of the end-effector and the wrench are recorded. The deformation of the robot components, including the end-effector, under the exerted external load is simply obtained by comparing the frames in initially unloaded and in loaded condition.

C. Stiffness Identification Result

The stiffness identification is carried out in four different robot configurations and the 6 DoF deformations are measured for each joint. Figure 2a shows the 6 DoF displacements of the origin of joint 4, i.e. displacements and rotation along and around x-, y-, and z-axis which is

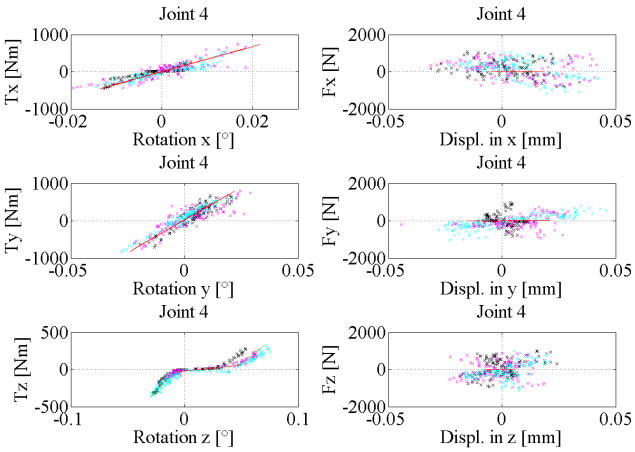

(a)

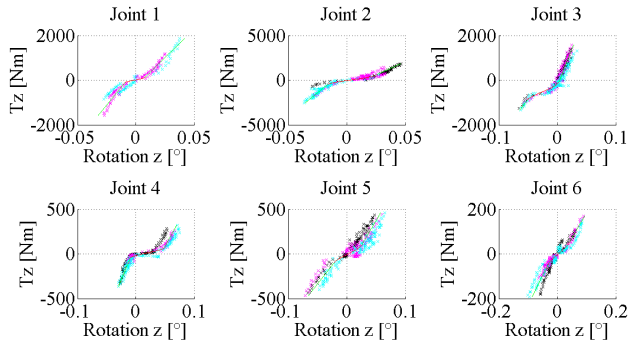

(b)

Fig. 2: 6D stiffness model of joint four including three rotations and three translations and b) rotational stiffness around z-axis of all six joints

the result of the linear least square fitting of the Eq. 1 for all four configurations (configurations are indicated by different colors). Due to the 6 DoF deformation all joints have impact on deformation of the position and orientation of the robot TCPs. This means that the stiffness matrix in the proposed method is not diagonal. External forces which are purely exerted on either x-, y-, or z-axis direction can cause deformation in all directions and orientations. It can also be seen that the linear least square fitting may not result to a very good model due to the disparity of the collected data in some joints. As a result, in order to increase the accuracy of the stiffness model, a non-linear least square fitting was

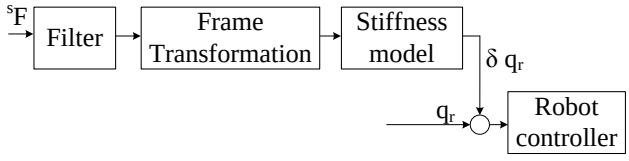

Fig. 3: Real-Time deformation compensation block diagram; ${}^sF$, δq_r and q_r represent the external force, deformation in reference, and reference joint angles, respectively.

used whenever required. It has to be noted that the main compliances of robotic joints are of rotational character, as there is a clear trend in rotational degrees of freedom x, y and z. Yet the displacements in translational directions only show amplitudes in the range of the measurement noises without any clear trend.

Figure 2b shows the dominant compliances of all six joints in the rotation around the z-axes. Note that the compliance function is a combination of compliance effects and backlash.

IV. DEFORMATION COMPENSATION

Figure 3 shows the block diagram of the real-time deformation compensation implemented in TwinCAT [18] for a KR 125 industrial manipulator of series 2000. The measurement noise has to be filtered out from force sensor data. Besides, the coordinate frame assigned to the force sensor is different from that of the robot base. As a result, the force sensor data is transformed to the robot base frame. On the other hand, in order to only deal with the external forces which are exerted to the end-effector due to the machining process, the weight of the force sensor, the fixture and the work piece are compensated. The deformation caused by machining forces is calculated in real-time using the model developed in Section II, and the joint references trajectory is recalculated by the robot controller. Consequently, the end-effector pose is modified. It should also be noted that the robot controller cycle time is 1 ms and hence, the deformation is calculated and fed to the controller every millisecond.

In order to verify the performance of the proposed deformation modeling and compensation, the performance is evaluated both in static and dynamic scenarios.

A. Static Performance

Using the same setup for stiffness identification, different loads are applied to the robot end-effector and the corresponding deformations in position and orientation are measured. The quality of the compliance model is demonstrated by two degrees of freedom in Figure 4a and Figure 4b showing the displacement along x-axis and around z-axis. Comparing the measured deformation and the calculated one, it can be seen that the the modeling errors along x-axis and around z- axis cause on the TCP an average of 0.1219 mm and $0.0161°$ over a range of around ± 1.5 mm and $\pm 0.25°$, respectively. The Cartesian deviation of the TCP shows an average of 0.4056 mm, for all captured measurements the Cartesian error can be specified to $<36\,\%$. It should also be noted that the calculated deformations in Fig. 4 are calculated with regard to the 6D deformation of each joint.

B. Dynamic Performance

To verify the dynamic performance of the proposed stiffness compensation different scenarios can be thought of such as applying an impulse load to the robot end-effector. The contact time, i.e. when the moment that the workpiece reaches the machining tool, can also be considered as an impulsive wrench and be used in evaluation of the dynamic performance of the stiffness compensation. Figure 5 shows

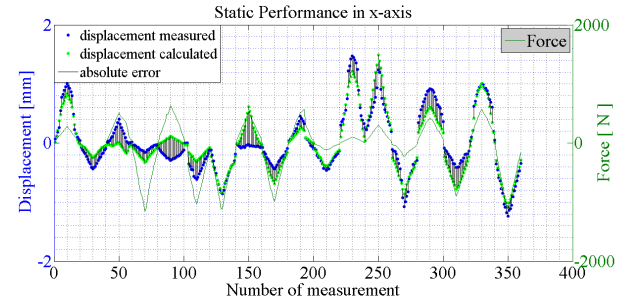

(a)

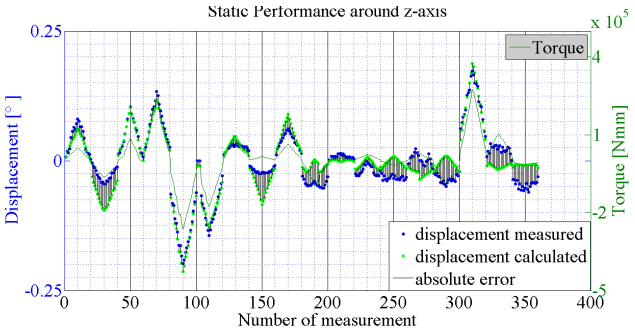

(b)

Fig. 4: Wrench-Deformation curve a) deformation along x-axis (Δx) and b) deformation around z-axis ($\delta\theta$) w.r.t the robot base frame

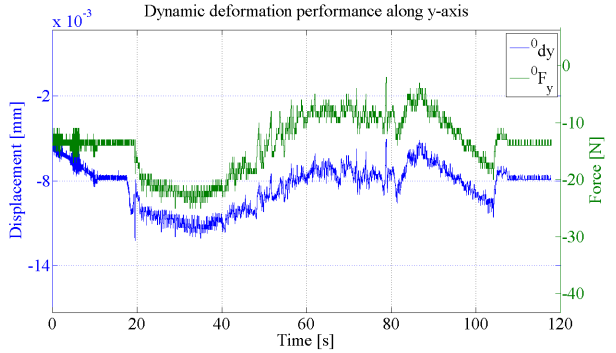

Fig. 5: Dynamic deformation response during the contact time: displacement in y-axis

the deformation response under such an impulsive wrench. As it can be seen, there is no compensation delay. On the other hand, it can be understood that even though the trend of the displacement along any of the axes has a direct relation with the applied force in that direction, it is also related to the forces applied in other directions. This is due to the off-diagonal elements in the stiffness matrix which also explains the coupling of the robot joints motion.

V. EXPERIMENTAL VALIDATION

In order to asses the effectiveness of the proposed deformation compensation method, milling tests on a steel block have been conducted. To this end, a Chopper 3300 spindle from Alfred Jaeger is used together with an 8 mm endmill

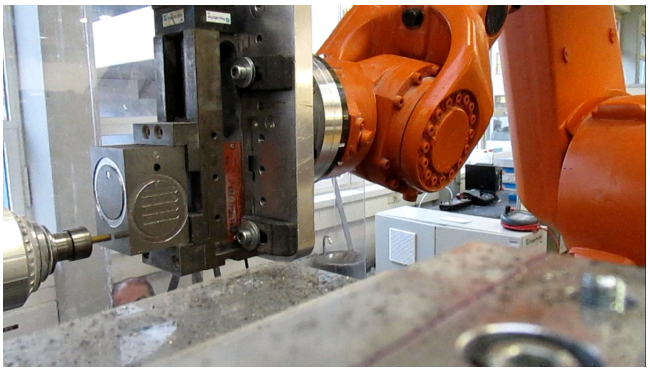

Fig. 6: Setup for machining with spindle and mounted force/torque sensor

Fig. 7: Circle machined in steel with compensation of deformation

tool with four teeth from Hoffman Group. The full setup is displayed in Figure 6. The purpose is to mill a circle of radius 35 mm (compare Figure 7).

Figure 8a shows the result of the machining measured with a Werth CMM of model Videocheck HA400 [19] while Fig. 8b shows the point-to-point error between the machined circle and the nominal circle. Although the normal contact force ${}^{s}F$ pushes the robot end-effector away from the metal block, the deformation compensation forces the robot to modify the end-effector and follow the desired path. Since the cutting force is significant in this setup, the overall effect is that there are still some point-to-point errors between the machined circle and the nominal one. The absolute average point-to-point error between the inner circles is 0.2 mm over 31.2 mm, the radius of the inner circle. Furthermore, it is clear that in some points there are larger errors and noticeable displacement in the machined circle from the nominal one. This is actually because of the left metal filings that has not been removed from the surface after the machining, in order to keep the experimental results as realistic as possible. A proper polishing could eliminate this problem which is out of the scope of this experiment. Having polished the surface, the point-to-point error and thus, the average error is reduced significantly.

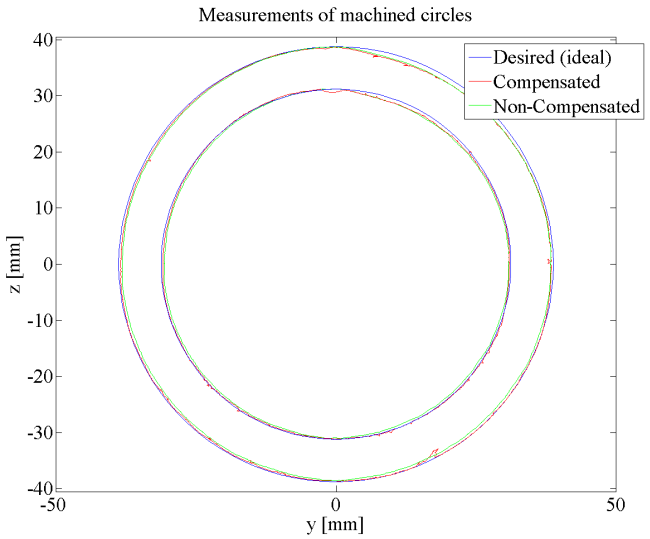

(a)

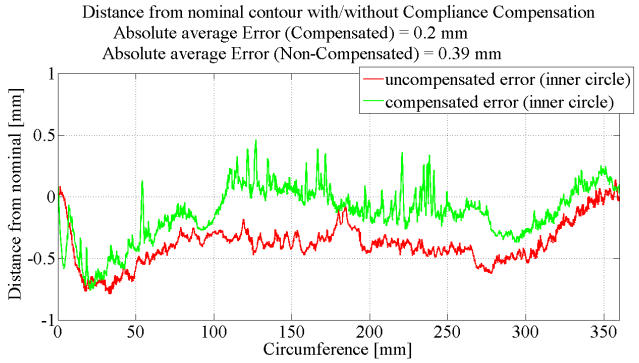

(b)

Fig. 8: Experimental results a) machined circle and b) point-to-point error

VI. CONCLUSIONS

In this paper the modeling, identification and robot deformation compensation caused by external process forces from the machining application are covered in detail. The experimental results show that the proposed method, which is indeed a feed forward model based compensation, can significantly reduce the error caused by robot deformation. Although robot deformation compensation is theoretically feasible, there are still a lot to do in order to see successful stories of robot machining applications in industry. The main challenges on this road are 1) how to simplify the stiffness identification process while its accuracy is preserved, 2) how to deal with the possible time delay between measuring the external force, calculating the corresponding deformation and modifying the robot end-effector position which is a question of optimisation of the speed of the robotic machining and the accuracy, and 3) how to deal with the entry and exit points where the robot is under some impulsive wrenches which is a matter of how dynamic the stiffness compensation should be. The future work of this research would be dealing with the entry and exit points together with modifying the robot controller in order to reduce the point-to-point error further.

ACKNOWLEDGMENT

The authors would like to acknowledge Mr. Justus Kopp and Mr. Julian Ricardo Diaz Posada at Fraunhofer IPA for taking part in the laboratory experiments and the implementation.

REFERENCES

[1] U. Schneider, M. Ansaloni, M. Drust, F. Leali, and A. Verl, "Experimental investigation of error sources in robot machining," in *Flexible Automation and Inteligent Manufacturing (FAIM)*, 2013.

[2] S.Y. Nof (Editor), *Handbook of Industrial Robotics*. John Wiley & Sons, New York, 1985.

[3] AccessScience, "Mcgraw-hill dictionary of scientific and technical terms." `http://www.accessscience.com/Dictionary/`, 2003. [online].

[4] S. Hayati and M. Mirmirani, "Improving the absolute positioning accuracy of robot manipulators," *J. Robotic Systems*, vol. 2, pp. 397–413, 1985.

[5] W. Khalil, G. Garcia, and J.-F. Delgarde, "Calibration of the geometrical parameters of robots without external sensors," in *IEEE International Conference on Robotics and Automation (ICRA)*, pp. 3039–3044, 1995.

[6] A. Elatta, L. Gen, F. Zhi, Y. Daoyuan, and L. Fei, "An overview of robot calibration," *Information Technology*, vol. 3, no. 1, pp. 74–78, 2004.

[7] E. Abele, M. Weigold, and S. Rothenbücher, "Modeling and identification of an industrial robot for machining applications," in *CIRP Annals – Manufacturing Technology*, pp. 387–390, 2007.

[8] J. Wang, H. Zhang, and T. Fuhlbrigge, "Improving machining accuracy with robot deformation compensation," in *IEEE/RSJ Int. Conf. on Intelligent Robots and Systems (IROS)*, pp. 3826–3831, 2009.

[9] C. Dumas, S. Caro, S. Garnier, and B. Furet, "Joint stiffness identification of six-revolute industrial robots," *Robotics and Computer-Integrated Manufacturing*, vol. 27, no. 4, pp. 881–888, 2011.

[10] Z. Pan and H. Zhang, "Improving robotic machining accuracy by real-time compensation," in *ICROS-SICE International Joint Conference*, pp. 4289–4294, IEEE, 2009.

[11] T. Oiwa, "Error compensation system for joints, links and machine frame of parallel kinematics machines," *Int. J. Robotics Research*, vol. 24, no. 12, pp. 1087–1102, 2005.

[12] U. Schneider, J. D. Posada, M. Drust, and A. Verl, "Position control of an industrial robot using an optical measurement system for machining purposes," in *Proceedings of the* 11^{th} *International Conference on Manufacturing Research (ICMR)*, 2013.

[13] H. Zhang, J. Wang, G. Zhang, Z. Gan, Z. Pan, H. Cui, and Z. Zhu, "Machining with flexible manipulator: toward improving robotic machining performance," in *Proceedings of the IEEE/ASME International Conference on Advanced Intelligent Mechatronics*, pp. 1127–1132, 2005.

[14] J. Salisbury, "Active control of a manipulator in cartesian coordinates," in *Proceedings of the* 19^{th} *IEEE Conference on Decision and Control*, pp. 95–100, 1980.

[15] S.-F. Chen and I. Kao, "Geometrical approach to the conservative congruence transformation (cct) for robotic stiffness control," in *IEEE International Conference on Robotics and Automation (ICRA)*, pp. 544–549, 2002.

[16] Nikon Metrology, "K-series optical CMM solutions," 2010. Data sheet Optical_CMM_EN_0311.

[17] ATI Industrial Automation, *Six-Axis Force/Torque Sensor System - Installation and Operation Manual*, 1995.

[18] Beckhoff Automation GmbH, "Beckhoff information system, TwinCAT 2," 2013. Verl, Germany.

[19] Werth GmbH, "CMM VideoCheck HA400," 2013. Gießen, Germany.